Heliyon 6 (2020) e05058

Contents lists available at ScienceDirect

Heliyon

journal homepage: www.cell.com/heliyon

Research article

Synthesis and potent antimicrobial activity of $CoFe_2O_4$ nanoparticles under visible light

Davood Gheidari [a,*], Morteza Mehrdad [a,*], Saloomeh Maleki [b], Samanesadat Hosseini [c]

[a] Department of Chemistry, Faculty of Science, University of Guilan, Iran
[b] Department of Chemistry, Faculty of Science, University of Shahrood, Iran
[c] Shahid Beheshti University of Medical Science, Tehran, Iran

ARTICLE INFO

Keywords:
Inorganic chemistry
Antibacterial
Escherichia coli
Staphylococcus aureus
Bacillus cereus

ABSTRACT

The nanoparticles of Cobalt ferrite are synthesized using polyethylene glycol as a solvent by the solvothermal method in a surfactant-free condition. Nanoparticles that were synthesized were determined by using various techniques such as Diffuse Reflection Spectroscopy (DRS), X-Ray Diffraction (XRD), Scanning Electron Microscope (SEM), and Energy Dispersive X-ray spectroscopy (EDAX). The Scanning electron microscope confirmed the range of spherical nanoparticles in the size of 20–33 nm.

An excellent match was observed between the calculated particles size in the X-ray diffraction and electron microscopes results. Furthermore, their antimicrobial efficacy was determined by MIC, MBC, IC50 and disc diffusion method on Gram-negative (*Pseudomonas aeruginosa* and *Escherichia coli*) and Gram-positive (*Staphylococcus aureus, Bacillus cereus*) bacteria. The results indicated an acceptable bacteriostatic and bactericidal effects of this nanoparticles. Additionally, it was seen that by the increase in the concentration of nanoparticles, their antimicrobial property would increase.

Background and objective: In recent years, antibacterial materials have found a special place to avoid the overuse of antibiotics. In this study, the antibacterial effects of $CoFe_2O_4$ nanoparticles on *Staphylococcus aureus, Escherichia coli, Pseudomonas aeruginosa, and Bacillus cereus,* were investigated due to their importance as human pathogens in nosocomial infection.

Methodology: In this study, the antibacterial effects of $CoFe_2O_4$ nanoparticles such as MIC, MBC, IC50, and disc diffusion method were examined.

Findings: According to the results, $CoFe_2O_4$ nanoparticles exhibited potent antibacterial activity against the bacteria that were examined, especially *Bacillus cereus*. The MBC (Minimum Bactericidal Concentration) of $CoFe_2O_4$ nanoparticle on *Escherichia coli*, *Staphylococcus aureus*, *Pseudomonas aeruginosa*, *Bacillus cereus* was between 0.12-0.48 mg/ml and MIC (Minimum Inhibition Concentration) on these bacteria detected between 0.06-0.24 mg/ml. The least IC50 determined for *Bacillus cereus* with a concentration of 0.061 mg/ml. *Pseudomonas aeruginosa* and *Bacillus cereus* identified as the most resistant and sensitive bacteria in the disc diffusion method, respectively.

1. Introduction

Recently, magnetic nanoparticles have attracted substantial consideration in the field of biomedicine because of their beneficial magnetic, optical, and antibacterial features at the Nanoscale. Ferrites, one of the most substantial magnetic materials, consist of two inverse and normal spinel structures. The spinel structure in cobalt ferrite is inverse and has various advantages such as good coupling efficiency, high magnetostrictivity and low cost [1]. Several applications are mentioned for Cobalt ferrite, such as magnetic resonance imaging (MRI), magnetic thermo-drug delivery hyperthermia, catalytic treatment of gases, oxidation of alkanes, drugs delivery, biosensors and gas detectors [2].

Of all different spinel ferrites, $CoFe_2O_4$ has attracted special attention on account of its unique physical features, including high Curie temperature, large magneto crystalline anisotropy, high coactivity, excellent chemical stability, large magnetostrictive coefficient, mechanical hardness and, moderate saturation magnetization [3]. The other advantage of $CoFe_2O_4$ nanoparticles is one order higher of magnetocrystalline anisotropy compared to other reported metal ferrite nanoparticles with the same saturation magnetization. Thus, the relaxation time of magnetic

* Corresponding authors.
E-mail addresses: davoodgheidari@phd.guilan.ac.ir, davoodgheidari@gmail.com (D. Gheidari), m-mehrdad@guilan.ac.ir (M. Mehrdad).

https://doi.org/10.1016/j.heliyon.2020.e05058
Received 16 July 2020; Received in revised form 13 September 2020; Accepted 21 September 2020
2405-8440/© 2020 The Authors. Published by Elsevier Ltd. This is an open access article under the CC BY-NC-ND license (http://creativecommons.org/licenses/by-nc-nd/4.0/).

$CoFe_2O_4$ nanoparticles is much lower than other metal ferrite nanoparticles with similar particle size [4, 5]. The specific surface area in Iron oxide nanoparticles is so high that they can interact with the surface structures of bacteria. In addition, since they are fairly small in size, they can expedite the particle uptake by bacterial cells. Various physicochemical methods are used to produce the iron oxide nanoparticles [6, 7]. Metal ferrite nanoparticles indicate substantial antibacterial activities. Of these metal ferrites, biocompatibility in cobalt ferrite nanoparticles are shown to be high, and their antibacterial activity makes them an appropriate option for antibacterial uses in industrial and medical fields [8]. Cobalt ferrite NPs cause toxic reactions (genotoxicity and cytotoxicity) in humans, organisms [9], and mice [10]. $CoFe_2O_4$ NPs induce oxidative stress in the liver (human & mice), human lungs, intestine, kidney, primary mouse dendritic-cells, and lymphoblast [9, 10]. These interactions with other organic materials and the type of toxicity are determined based on their physicochemical properties and unique compositions (charge, size, purity, shape, colloidal stability, and inertness, etc.) [11]. The particles of Iron oxide are already understood to be nonhazardous magnetic materials, and also MRI contrast agents have already been proved as harmless for human use [12].

In reduction and oxidation procedures, Photo-catalysts are significant materials offering a pretty simple tool to convert solar energy for use. Photo-catalysis is used in various fields, such as cancer cells and bacterial inactivation, contaminants elimination from water and air, etc. [13, 14, 15, 16, 17]. Having a general formula of MFe_2O_4, Spinel ferrites are magnetic materials that are chemically and thermally stable and utilized for many applications [18, 19]. In this formula, M represents a metal cation. Ferrites have important photo-catalytic properties for numerous industrial processes [19], ranging from hydrogen peroxide and alcohols decomposition [20] to the oxidative dehydrogenation of hydrocarbons [21] and the oxidation of compounds like CO [22]. The features of the ferrites highly rest on elements including the site, nature, and amount of metal used in the structure [18]. As an example, the redox properties of the ferrites are intensely modified by the replacements of transition metals such as Ni^{+2}, Cu^{+2} [23], or Co^{+2} [24] into the spinel lattice. Ferrites offer the benefit of having a band gap able to absorb visible light, as well as the spinel crystal structure, which enhances efficiency owing to the existing additional catalytic sites by means of the crystal lattice [25]. Generally, Ferrites of the form MFe_2O_4 consist of metal cations such as Ca^{2+} [26], Co^{2+} [20, 27, 28], Fe^{2+} [19, 27, 28, 29].

Today, due to the significant role of microorganisms in the development of various diseases and at the same time increasing antibiotic resistance following the excessive use of antibiotics, it is essential to find effective and new substances that have potent antibacterial impacts. Constant study will also be very important to the antibacterial effects of these substances in different regions against various bacterial strains for the epidemiological aspects. The importance of determining the antibacterial effects of these substances would be much greater when we know excessive costs are spent on the design and manufacture of antibiotics and other disinfectants in the world, annually.

In this investigation, Magnetic cobalt nanoparticles were synthesized by utilizing a solvothermal method and polyethylene glycol applied as solvent with no presence of surfactants. Polyethylene glycol (PEG) are applied to coat and stabilize cobalt nanoparticles which, in turn, reducing the toxicity of the nanoparticles. Besides, the metal salts extremely dissolve in this solvent. In the last decade, the implementation of nanomaterials was comprehensively expanded. Physical and chemical properties of nanomaterial are various from large bulk [30, 31]. The possibility of the adsorption, interacting, and reacting enhance between nanoparticles and other atoms and molecules because of enhancing atoms proportion placed at the surface [31, 32]. Antibacterial activity of $CoFe_2O_4$ in the existence of visible white light gives a faster inhibition of bacterial growth as a result of the higher quantum yields. These alternative nanoparticles could dominate the disadvantages associated with Fe^{2+} by applying the solid form of iron instead of Fe^{2+} as iron salts.

As shown in Eqs. (1) and (2) [33, 34], when the iron oxides are susceptible to white light irradiation, consequently the photo-reduction of ferric to ferrous ions and generation of $^{\bullet}OH$ radicals are increased which reduces bacterial growth.

$$Fe(OH)_2+ + h\upsilon \rightarrow Fe\ (II) + OH \quad (1)$$

$$Fe\ (III) + H_2O + h\upsilon \rightarrow Fe\ (II) + H^+ + {}^{\bullet}OH \quad (2)$$

Irradiation of photons with energy (higher than 3.2 eV) to the iron oxides causes electron excitation from the valence band to the conduction band [35]. Furthermore, the hydroxyl, perhydroxyl, and superoxide anion radicals can be procreated by the reaction between the dissolved oxygen and electrons [36] that increases inhibition of bacterial growth. The attack of hydroxyl radicals to the bacterial cell wall obviously lead to breakage of structures. The results of this study confirmed that $CoFe_2O_4$ nanoparticles could have efficient antibacterial properties against bacterial pathogens, especially *bacillus cereus*. on the other hand, we also found that, the inhibitory effect of $CoFe_2O_4$ on bacterial growth will be increased if nanoparticle's concentration increased (from 0.06-0.48 mg/ml). This evidence is similar to another study, that carried out by Sanpo et al. in 2013, which explored the antibacterial effect of $CoFe_2O_4$ on *Staphylococcus aureus* and *Escherichia coli* [8]. They also revealed that $CoFe_2O_4$ nanoparticle's inhibitory effect on *Escherichia coli* is higher than *Staphylococcus aureus*, which these results besides other research are in line with the outcomes of our study [8, 37, 38, 39]. One of the impressive results from this study is the same sensitivity of *Staphylococcus aureus* to a lower concentration of the nanoparticle compares to research in which the higher concentration of this nanoparticle was used, indicates an advance in antibacterial potency of $CoFe_2O_4$ nanoparticles through the used methods.

Another mechanism that causes nanoparticle's antibacterial activity is the discharge of reactive oxygen species (ROS) such as superoxide (O_2) and hydrogen peroxide (H_2O_2) from the surface of nanoparticles [40, 41]. Thus, active oxide amounts have an efficient role in bacterial eliminating by nanoparticles through the penetration in their cell wall [42]. Furthermore, Chung et al. suggested that the accumulation of negative charge on the gram-negative bacterial cell wall is more than gram-positive bacteria. Accordingly, the interaction of nanoparticles which have a positive charge with the bacterial cell wall that has a negative charge leads to leakage of the bacterial cell contents [43]. Thus, we propose $CoFe_2O_4$ nanoparticles as a useful antibacterial agent for future investigations on clinical specimens, that their impacts also can develop by using these effective methods.

2. Experimental

2.1. Chemistry and materials

Starting materials of Polyethylene glycol (>99%), $FeCl_3$ (>99%), $CoCl_2$ (>99%), and $C_2H_3NaO_2$ (>99%) of analytical grade were provided by Merck Co.

2.1.1. $CoFe_2O_4$ synthesis

In this project, the solvothermal method was utilized in the synthesis of Cobalt ferrite magnetic nanoparticles by dissolving 2 g polyethylene glycol in 30 ml of distilled water and stirring for 10 min by a magnetic stirrer to prepare a clear solution at room temperature. Then, specific amounts of dehydrating iron (III) chloride, cobalt chloride, and sodium acetate were added to the solution, and to make the mixture homogeneous, it was stirred for about 2 h by means of a magnetic stirrer. The solution was placed in the furnace and dried at 190 °C for 15 h. After cooling the solution, it was filtered and then washed with double distilled water and ethanol 96% several times. The precipitates were dried completely for 24 h and then the powders were placed at 450 °C for 2 h in the furnace to obtain $CoFe_2O_4$ magnetic nanoparticles (Figures 1 and 2).

2.2. Pharmacology

Bacillus Cereus (PTCC1015), *Staphylococcus aureus* (PTCC1112), *Pseudomonas aeruginosa* (PTCC 1074) and *Escherichia coli* (PTCC 1399) used for antibacterial examination. These bacteria were cultured on specific media, including DNase, Mannitol Salt Agar, MacConkey Agar and Blood Agar. Assuring the identification of bacteria were done due to the biochemical tests after 24 h incubation at 37 °C, then the specimens were used to prepare bacterial suspension [44]. 1.5×10^8 CFU/ml bacterial inoculum was prepared using a spectrophotometer at 620 nm [26]. First, 50 μl of Trypticase Soy Broth and bacterial inoculum added into each well that was included difference concentrations of two-fold diluted nanoparticles ranging from 0.96 mg/ml to 0.001 mg/ml in the wells then 96-well plates incubated at 37 °C for 18–24 h under 18-volt white light at a distance of 33 cm. Likewise, for IC50 value detection, the concentration of the antibacterial agent which inhibits 50% of bacterial growth, the above procedure was done and turbidity of each well was read to 3 times by ELISA READER stat fax 2100 and the data analyzed by GraphPadPrism 6.05, subsequently. The MBC also determined using plate culture in Mueller-Hinton agar from no bacterial growth shown concentrations of nanoparticle in the MIC test. To observe the antibacterial activity of nanoparticle in the disc diffusion method [45], 100μl of bacterial inoculum that was prepared like previously, streaked on Mueller Hinton Agar surface by the swab. Then the impregnated discs with different concentrations of nanoparticle include 0.06, 0.12, 0.24 and 0.48 mg/ml that was provided in 50 μl DMSO as a solvent, positioned on the surface of the injected agar plate. Notably, the blank disc with any nanoparticle was used for control. Finally, The Plates incubated at 37 °C for 24 h under 18-volt white light at a distance of 33 cm, and the results recorded by measuring the diameter of the growth inhibition zone.

3. Results and discussion

3.1. XRD analysis

Using X' Pert Pro system from the Panalytical company, X-ray diffraction patterns of $CoFe_2O_4$ were reported under the following conditions: 40 mA, 40 kV, step size: 0.02, and timer per step 1 s/step and showed that there are no additional peaks in the XRD patterns. Bragg reflections were reported in the 2θ range of 5–80, ensuring purity. The analyses of qualitative phase, quantitative phase, and study of preferred orientation of synthetized powder sample illustrate in X-ray diffraction profile. X-ray diffraction schema of $CoFe_2O_4$ is shown in Figure 3. As shown in the figure, the peaks at 2θ values of 30.19°, 35.532°, 43.17°, 53.54°, 57.087°, 62.682° and 74.20° were respectively corresponded to 226, 778, 185, 92, 265, 424, and 86 reflections of $CoFe_2O_4$. All 2θ X-ray diffraction (XRD) observed in this study consistent with reports from other researchers concerning the synthesis of $CoFe_2O_4$ [3,46-48]. The remarkable property was that no impurity phase was observed in the synthetized powders [49, 50, 51].

The reflected peaks of the sample had the same position as a cubic unit cell, corresponding to an inverse spinel structure of cobalt ferrite nanoparticles (JCPDS No. 98-011-1281). Crystallite sizes of $CoFe_2O_4$ obtained by statistical analysis of XRD in Table 1.

Crystallite sizes of $CoFe_2O_4$ reported 309 [Å] (30.9 nm) using Debye Scherrer,

$$T = K \times \lambda / \beta \, Cos\Theta \quad (3)$$

Where T is crystallite size, K is Scherrer constant, λ is the wavelength of the X-ray, β is full-width half-maximum of the plane, and Θ is the Bragg angle. The particle size and their distribution are detected to be almost nearly spherical and uniform in the sample; therefore, it can be use fixed K value in the equation. Examination of X-ray pattern shows that the peaks are consistent with standard pattern with the number completely, which indicates that specimens are pure and they have very well crystallinity.

Figure 1. Powder of $CoFe_2O_4$ nanoparticles.

3.2. EDX analysis

Using Oxford, instrument EDX analysis indicated pure $CoFe_2O_4$ nanoparticles formation; Figure 3 shows an illustration of the samples.

No significant discrepancy was detected in nanoparticles size, and almost all particles had a spherical shape. The EDX spectral analysis of the synthesized $CoFe_2O_4$ nanoparticles composition illustrates in Figure 4. The ratio of the EDX peaks represent the expected elemental composition of synthetized nanoparticles. The synthetized product consists of only three elements namely Co, Fe, O. Thus, it can be resulted that the achieved nanoparticles do not contain of any other impurities. The strong peaks of Fe display the EDX spectra. The composition analysis indicates 59.6% Fe, 14.4% O_2 and 26.0% cobalt, illustrating the high purity of $CoFe_2O_4$ nanoparticles. The atomic ratio of cobalt to iron was obtained 0.4362, which is near to the stoichiometric value of 0.5 [52-53]. The sample preparation and analysis procedures to cover it with Au, generate conductivity and electric charge flow explain the existence of Au peak in the EDX analysis spectral.

3.3. FE-SEM analysis

E-SEM measurements of sample $CoFe_2O_4$ were reported using the SIGMA VP model system from ZEISS Company. They showed a uniform distribution of spherical nanoparticles. Figure 4 and Figure 5 represent FE-SEM morphology.

The images of cobalt ferrite magnetic nanoparticles in various scales achieved using SEM technique are shown in Figure 5(a,b) respectively. It is explicit in the figures that the particle size of the $CoFe_2O_4$ is at nano scale. The nanoparticle size was measured approximately spherical which had uniform distribution in the sample. The average particle size specified from SEM images is remarked as 22–46 nm for $CoFe_2O_4$ which is nearly agreement with the size determined from XRD data. As concluding from SEM analysis, the agglomeration due to the magnetic force results in non-uniform and heterogeneous morphology of $CoFe_2O_4$ particles.

3.4. Diffuse Reflection Spectroscopy (DRS) of $CoFe_2O_4$

The semiconducting materials, which can explain the quantum size effect of the nanoparticles by the absorption edge, were described using this information. The optical characteristics of $CoFe_2O_4$ nanoparticles were examined in the range of 200–800 nm, which is shown in Figure 6.

The F® value presents the reflectance data, acquired by the application of the Kubelka-Munk method, Where R is the measured reflectance. The bandgap energy value of the $CoFe_2O_4$ is 1.85 eV. In order to

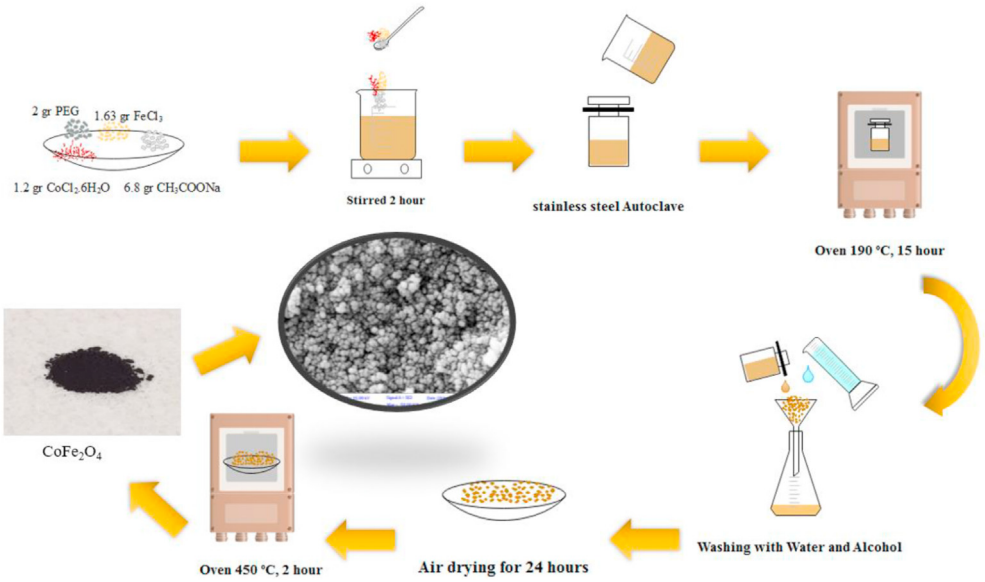

Figure 2. $CoFe_2O_4$ nanoparticles synthesized with solvothermal method.

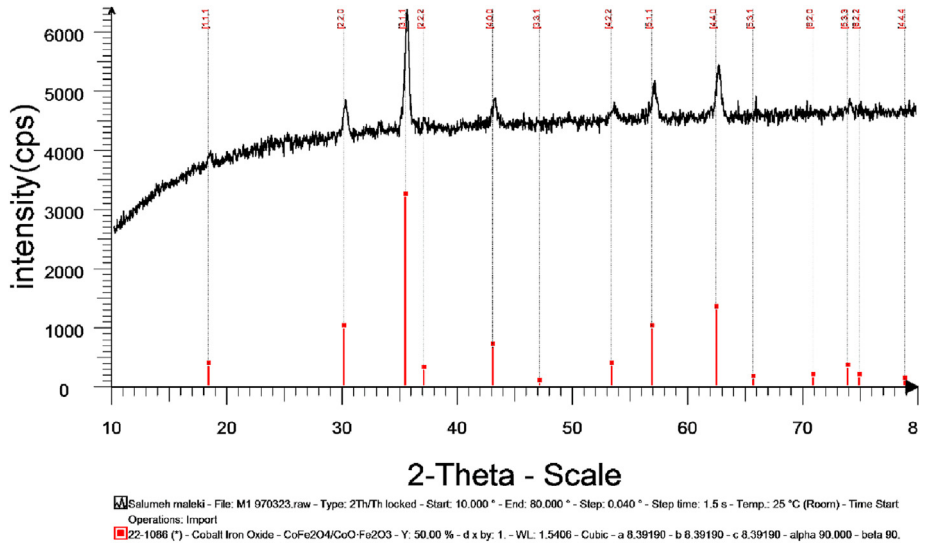

Figure 3. X-ray diffraction patterns of $CoFe_2O_4$.

determine the semiconducting materials that explain the quantum size effect of the nanoparticles by absorption edge, we used this information. Light was transmitted in the visible region by this nanoparticle.

3.5. Cytotoxicity of $CoFe_2O_4$ nanoparticles

The cytotoxicity of $CoFe_2O_4$ nanoparticles was measured by analyzing the cell survival MTT assay utilizing ELISA READER after 24 h incubation at 0.06 mg/ml and 0.48 mg/ml concentrations. The analysis indicated a survival rate of more than 50% for the maximum concentration of 0.06 mg/ml. Based on the results of previous studies demonstrated the cytotoxicity of $CoFe_2O_4$ nanoparticles of almost 90% for the maximum concentration of 0.75 and 1 mg/ml [54, 55], the achieved data represented that the synthesized $CoFe_2O_4$ nanoparticles led to concentration-dependent cell death where the enhancement in concentration involved a remarkable reduction in cell proliferation. . In addition, the estimated IC50 value was detected to be 0.06 mg/ml.

3.6. Antimicrobial activity of $CoFe_2O_4$

According to the results, the most sensitive bacteria that have investigated in this study against the nanoparticle is *Bacillus cereus*. As well as, *Pseudomonas aeruginosa and Staphylococcus aureus* detected as the most resistant bacteria, bothy (Table 2). Furthermore, based on the results, as the concentration of nanoparticles increased, the bacterial population would decrease compared to the control plate.

Table 1. Crystallite sizes of $CoFe_2O_4$.

No	B obs. [°2Th]	B std. [°2Th]	Peak pos. [°2Th]	B struct. [°2Th]	Crystallite size [Å]
1	0.36	0.09	35.532	0.27	309

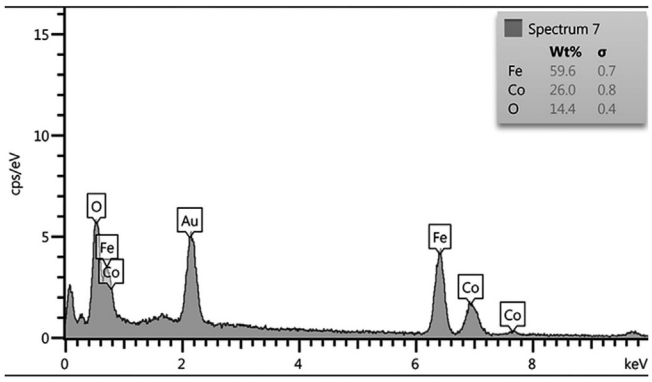

Figure 4. EDX spectrum of $CoFe_2O_4$ with percentage of elements.

The encouraging antibacterial potential of $CoFe_2O_4$ nanoparticles at different concentrations were corroborated by results of experiments the antibacterial activity of the synthesized $CoFe_2O_4$ nanoparticles. Furthermore, a large ratio of surface to volume raises the antibacterial activity of metal nanoparticles [56]. In our investigation, the obtained results demonstrated that the IC50 values of the synthesized $CoFe_2O_4$ nanoparticles was determined 0.06 mg/ml and the IC50 index by confirming the other antibacterial tests indicates the required nanoparticle's concentration to inhibit 50% of bacterial growth. This is in accordance with the results of several investigations with various metal nanoparticles. The authors reported that maximum inhibition of 57.74% was resulted at 0.1 mg ZnONPs/ml [57]. Moreover, the antioxidant activity of the chemically synthesized ZnONPs with 33% inhibition at 0.025 mg ZnONPs ml was achieved by Abd Elkodous et al [58]. Abdelhakim et al. reported that the attained IC50 of the synthesized ZnONPs was 0.1023 mg/ml [59]. In accordance with our findings, El-Sayed et al reported that $CoFe_2O_4$ nanoparticles concentration dependent activity against human breast and liver cancer cell lines was illustrated by the MTT cytotoxicity assay. That metal nanoparticles synthesized by the fungus *Monascus purpureus* ATCC16436, had a single-phase crystalline structure and spherical shape with particle size of 6.50 nm. The synthesized $CoFe_2O_4$ nanoparticles represented antibacterial potential with 50% inhibitory concentration of 0.10025 mg/mL [60]. Besides, the antioxidant, anticancer and antimicrobial activities of Selenium nanoparticles (SeNPs) synthesized by the culture extract of fungus grown on sugarcane bagasse under solid-state fermentation were evaluated. The SeNPs displayed spherical shape by the particle size of 46.58 nm and antioxidant activity with 50% inhibitory concentration of 0.08592 mg/mL as well as previous investigation by these authors [61]. Thus, the reported antibacterial property of $CoFe_2O_4$ nanoparticles in this research will open up the new way to the application of $CoFe_2O_4$ nanoparticles as a new source of antibacterial.

The disc diffusion test showed the same result with other antibacterial tests, specially IC50 determining value as showed in Table 3, *Pseudomonas aeruginosa* detected as the most resistant bacteria in 0.48 mg/ml concentration of this nanoparticle with a 12 mm diameter of growth inhibition zone. Furthermore, the most sensitive bacteria were *Bacillus cereus* with a 12 mm diameter of growth inhibition zone in 0.06 mg/ml concentration of this nanoparticle.

3.7. Photocatalytic activity of $CoFe_2O_4$ nanoparticles

$CoFe_2O_4$ nanoparticles have been employed for white light driven antimicrobial and photocatalytic activity. The photocatalytic behavior of the synthesized $CoFe_2O_4$ nanoparticles against *Bacillus Cereus*, *Staphylococcus aureus*, *Pseudomonas aeruginosa*, and *Escherichia coli* was explored after 24 h being exposure white light to attain equilibrium. The bacterial degradation in the presence of $CoFe_2O_4$ nanoparticles was confirmed by measuring the diameter of the growth inhibition zone. The bacterial inactivation of this nano-catalyst achieved 50% under white light for 24 h, much higher than without light. Figure 7 illustrates pictures of $CoFe_2O_4$ nanoparticles treated with *Bacillus Cereus*, *Staphylococcus aureus*, *Pseudomonas aeruginosa*, and *Escherichia coli* in the dark and under white light for 24 h. Bacteria grow into colonies on these samples in the dark. $CoFe_2O_4$ nanoparticles can inactivate bacteria by irradiating with white light for 24 h. The degradation rate of bacteria was increased in the presence of $CoFe_2O_4$ nanoparticles as catalysts under visible light in comparison without exposure. Hence, it is predicted that $CoFe_2O_4$ nanoparticles will cause many possibilities for producing more novel nano dimensional metal including compounds with numerous functionalities.

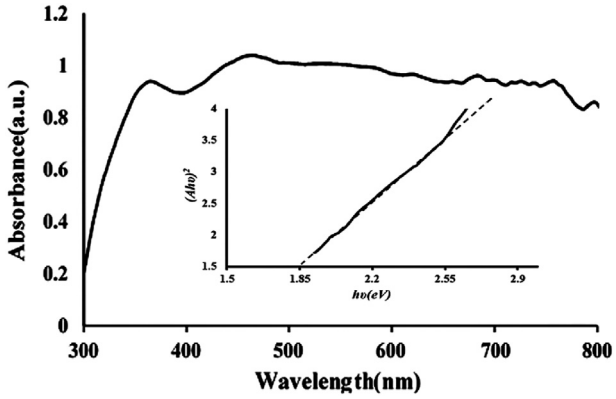

Figure 6. Diffuse Reflection Spectroscopy and UV-visible diffuse reflectance spectra of $CoFe_2O_4$ nanoparticles.

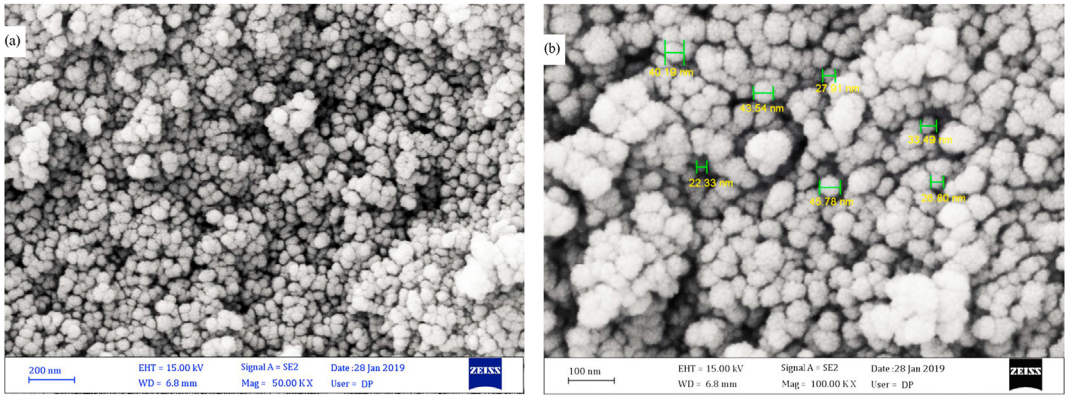

Figure 5. (a,b). (a) FE-SEM image of $CoFe_2O_4$ on a scale of 200 nm and (b) FE-SEM image of $CoFe_2O_4$ on a scale of 100 nm with higher magnification.

Table 2. Amounts of MIC, MBC and IC50 of $CoFe_2O_4$ nanoparticle against bacteria.

Bacteria	MIC (mg/ml)	IC50 (mg/ml)	MBC (mg/ml)
Escherichia coli	0.12	0.08	0.24
Staphylococcus aureus	0.24	0.16	0.48
Pseudomonas aeruginosa	0.24	0.18	0.48
Bacillus cereus	0.06	0.06	0.12

Table 3. Bacterial growth inhibition zone (mm) based on the nanoparticle concentration.

Bacteria	Concentrations(mg/ml)			
	0.48	0.24	0.12	0.06
Bacillus cereus	20	16	14	12
Pseudomonas aeruginosa	12	11	10	8
Escherichia coli	18	14	12	11
Staphylococcus aureus	13	12	11	9

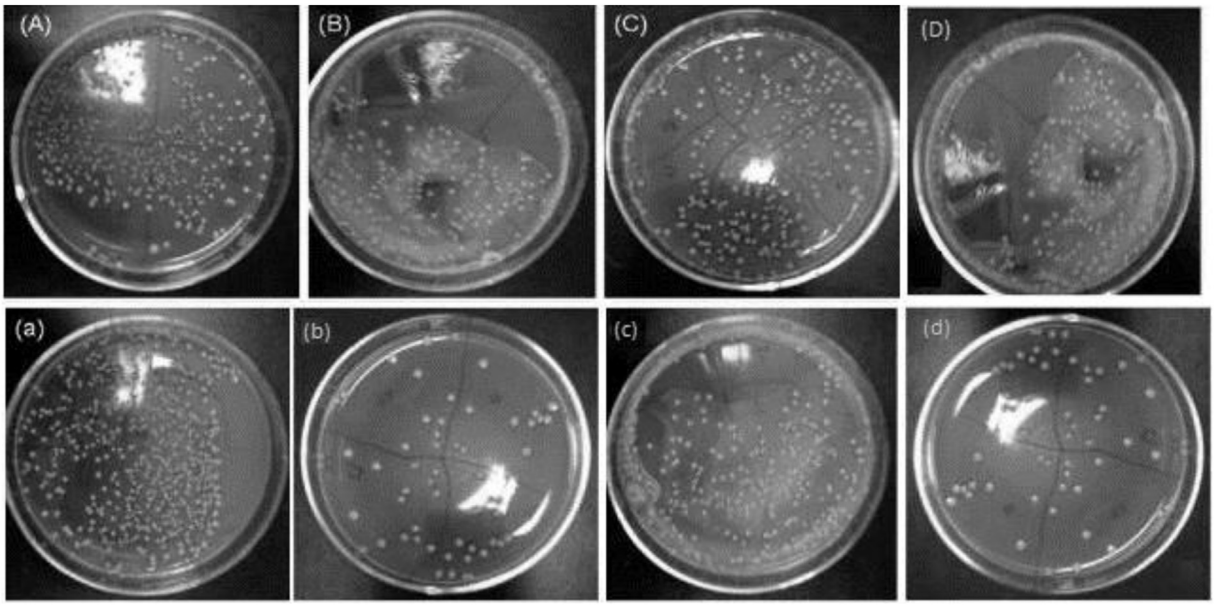

Figure 7. Pictures of bacteria colonies developed on agar plates treated (A) *Bacillus Cereus*, (B) *Staphylococcus aureus* and (C) *Escherichia coli*, and (D) *Pseudomonas aeruginosa* without white light. (a) *Bacillus Cereus*, (b) *Staphylococcus aureus* and (c) *Escherichia coli*, and (d) *Pseudomonas aeruginosa* are the images of bacteria colonies under white light irradiation for 24h.

4. Conclusion

In this study, $CoFe_2O_4$ nanoparticles were synthesized through the solvothermal method. The properties of $CoFe_2O_4$ nanoparticles were analyzed by Scanning Electron Microscopy (SEM), Energy Dispersive X-ray spectroscopy (EDX), X-Ray Diffraction (XRD), and Diffuse Reflection Spectroscopy (DRS). Furthermore, MIC and MBC and antimicrobial activity were tested under visible light against Gram-positive (*Staphylococcus aureus and Bacillus cereus*) and Gram-negative (*Pseudomonas aeruginosa* and *Escherichia coli*) bacteria with different weight nits of $CoFe_2O_4$. One of the effective results from this work is the same sensitivity of *Staphylococcus aureus* to a lower concentration of the nanoparticle compares to the study in which the higher concentration of this nanoparticle was carried out, shows a progress in antibacterial potency of $CoFe_2O_4$ nanoparticles through the utilized methods. Also, the obtained results demonstrated that the IC50 values of the synthesized $CoFe_2O_4$ nanoparticles was determined 0.06 mg/ml and the IC50 index by confirming the other antibacterial tests indicates the required nanoparticle's concentration to inhibit 50% of bacterial growth. So, the nanoparticles showed good potency against all of the microorganisms which were used in this study.

Declarations

Author contribution statement

Morteza Mehrdad: Conceived and designed the experiments; Performed the experiments; Contributed reagents, materials, analysis tools or data.

Samanesadat Hosseini: Conceived and designed the experiments; Performed the experiments.

Davood Gheidari: Conceived and designed the experiments; Performed the experiments; Analyzed and interpreted the data; Wrote the paper.

Saloomeh Maleki: Conceived and designed the experiments; Performed the experiments; Analyzed and interpreted the data.

Funding statement

This work was supported by the University of Guilan.

Competing interest statement

The authors declare no conflict of interest.

Additional information

No additional information is available for this paper.

Acknowledgements

I would like to give special thanks to Mr. Akbar Gheidari, Ms. Zarafshan Saeidi, my Sisters and Brothers for their continuous help, support and encouragement.

References

[1] K. Kombaiah, J.J. Vijaya, L.J. Kennedy, M. Bououdina, R.J. Ramalingam, H.A. Al-Lohedan, Okra extract-assisted green synthesis of $CoFe_2O_4$ nanoparticles and their optical, magnetic, and antimicrobial properties, Mater. Chem. Phys. 204 (2018) 410–419.

[2] Y. Hammiche-Bellal, A. Djadoun, L. Meddour-Boukhobza, A. Benadda, A. Auroux, M.-H. Berger, F. Mernache, Effect of the preparation method on the structural and catalytic properties of spinel cobalt-iron oxide, Mater. Chem. Phys. 177 (2016) 384–397.

[3] A.B. Rajput, S. Hazra, N.N. Ghosh, Synthesis and characterisation of pure single-phase $CoFe_2O_4$ nanopowder via a simple aqueous solution-based EDTA-precursor route, J. Exp. Nanosci. 8 (4) (2013) 629–639.

[4] I. Malinowska, Z. Ryżyńska, E. Mrotek, T. Klimczuk, A. Zielińska-Jurek, Synthesis of $CoFe_2O_4$ nanoparticles: the effect of ionic strength, concentration, and precursor type on morphology and magnetic properties, J. Nanomater. 2020 (2020).

[5] L. Ai, J. Jiang, Influence of annealing temperature on the formation, microstructure and magnetic properties of spinel nanocrystalline cobalt ferrites, Curr. Appl. Phys. 10 (1) (2010) 284–288.

[6] R. Hufschmid, H. Arami, R.M. Ferguson, M. Gonzales, E. Teeman, L.N. Brush, N.D. Browning, K.M. Krishnan, Synthesis of phase-pure and monodisperse iron oxide nanoparticles by thermal decomposition, Nanoscale 7 (25) (2015) 11142–11154.

[7] W. Glasgow, B. Fellows, B. Qi, T. Darroudi, C. Kitchens, L. Ye, T.M. Crawford, O.T. Mefford, Continuous synthesis of iron oxide (Fe_3O_4) nanoparticles via thermal decomposition, Particuology 26 (2016) 47–53.

[8] N. Sanpo, C.C. Berndt, C. Wen, J. Wang, Transition metal-substituted cobalt ferrite nanoparticles for biomedical applications, Acta Biomater. 9 (3) (2013) 5830–5837.

[9] L. Horev-Azaria, G. Baldi, D. Beno, D. Bonacchi, U. Golla-Schindler, J.C. Kirkpatrick, S. Kolle, R. Landsiedel, O. Maimon, P.N. Marche, Predictive toxicology of cobalt ferrite nanoparticles: comparative in-vitro study of different cellular models using methods of knowledge discovery from data, Part. Fibre Toxicol. 10 (1) (2013) 32.

[10] D.S. Lee, S. Kim, Gene expression profiles for genotoxic effects of silica-free and silica-coated cobalt ferrite nanoparticles, J. Nucl. Med. 53 (1) (2012) 106–112.

[11] K. Luyts, D. Napierska, B. Nemery, P.H. Hoet, How physico-chemical characteristics of nanoparticles cause their toxicity: complex and unresolved interrelations, Environ. Sci. Process. Impact. 15 (1) (2013) 23–38.

[12] P.R. Ros, P.C. Freeny, S.E. Harms, S.E. Seltzer, P.L. Davis, T.W. Chan, A.E. Stillman, L.R. Muroff, V.M. Runge, M.A. Nissenbaum, Hepatic MR imaging with ferumoxides: a multicenter clinical trial of the safety and efficacy in the detection of focal hepatic lesions, Radiol. 196 (2) (1995) 481–488.

[13] C. Shifu, Z. Wei, L. Wei, Z. Huaye, Y. Xiaoling, Preparation, characterization and activity evaluation of p–n junction photocatalyst p-CaFe2O4/n-ZnO, Chem. Eng. J. 155 (1-2) (2009) 466–473.

[14] J. Kim, C.W. Lee, W. Choi, Platinized WO_3 as an environmental photocatalyst that generates OH radicals under visible light, Environ. Sci. Technol. Lett. 44 (17) (2010) 6849–6854.

[15] Y. Bi, S. Ouyang, N. Umezawa, J. Cao, J. Ye, Facet effect of single-crystalline Ag_3PO_4 sub-microcrystals on photocatalytic properties, J. Am. Chem. Soc. 133 (17) (2011) 6490–6492.

[16] W. Morales, M. Cason, O. Aina, N.R. de Tacconi, K. Rajeshwar, Combustion synthesis and characterization of nanocrystalline WO_3, J. Am. Chem. Soc. 130 (20) (2008) 6318–6319.

[17] P. Wang, B. Huang, X. Qin, X. Zhang, Y. Dai, J. Wei, M.H. Whangbo, Ag@ AgCl: a highly efficient and stable photocatalyst active under visible light, Angew. Chem. Int. Ed. 47 (41) (2008) 7931–7933.

[18] E. Casbeer, V.K. Sharma, X.-Z. Li, Synthesis and photocatalytic activity of ferrites under visible light: a review, Separ. Purif. Technol. 87 (2012) 1–14.

[19] D. Guin, B. Baruwati, S.V. Manorama, A simple chemical synthesis of nanocrystalline AFe_2O_4 (A= Fe, Ni, Zn): an efficient catalyst for selective oxidation of styrene, J. Mol. Catal. Chem. 242 (1-2) (2005) 26–31.

[20] E. Manova, T. Tsoncheva, D. Paneva, I. Mitov, K. Tenchev, L. Petrov, Mechanochemically synthesized nano-dimensional iron–cobalt spinel oxides as catalysts for methanol decomposition, Appl. Catal. Gen. 277 (1-2) (2004) 119–127.

[21] M.A. Gibson, J.W. Hightower, Oxidative dehydrogenation of butenes over magnesium ferrite kinetic and mechanistic studies, J. Catal. 41 (3) (1976) 420–430.

[22] S. PalDey, S. Gedevanishvili, W. Zhang, F. Rasouli, Evaluation of a spinel based pigment system as a CO oxidation catalyst, Appl. Catal., B 56 (3) (2005) 241–250.

[23] C. Ramankutty, S. Sugunan, B. Thomas, Study of cyclohexanol decomposition reaction over the ferrospinels, A1− $xCuxFe_2O_4$ (A= Ni or Co and x= 0, 0.3, 0.5, 0.7 and 1), prepared by 'soft'chemical methods, J. Mol. Catal. Chem. 187 (1) (2002) 105–117.

[24] R. Persoons, E. De Grave, On the Verwey transition in cobalt-substituted magnetite as determined by 57Fe Mössbauer spectroscopy, Solid State Commun. 72 (10) (1989) 977–980.

[25] R. Dom, R. Subasri, K. Radha, P.H. Borse, Synthesis of solar active nanocrystalline ferrite, MFe_2O_4 (M: Ca, Zn, Mg) photocatalyst by microwave irradiation, Solid State Commun. 151 (6) (2011) 470–473.

[26] J. McFarland, The nephelometer: an instrument for estimating the number of bacteria in suspensions used for calculating the opsonic index and for vaccines, J. Am. Med. Assoc. 49 (14) (1907) 1176–1178.

[27] P. Baldrian, V. Merhautová, J. Gabriel, F. Nerud, P. Stopka, M. Hrubý, M.J. Beneš, Decolorization of synthetic dyes by hydrogen peroxide with heterogeneous catalysis by mixed iron oxides, Appl. Catal., B 66 (3-4) (2006) 258–264.

[28] S. Zhang, H. Niu, Y. Cai, X. Zhao, Y. Shi, Arsenite and arsenate adsorption on coprecipitated bimetal oxide magnetic nanomaterials: $MnFe_2O_4$ and $CoFe_2O_4$, Chem. Eng. J. 158 (3) (2010) 599–607.

[29] S. Hatanaka, N. Matsushita, M. Abe, K. Nishimura, M. Hasegawa, H. Handa, Direct immobilization of fluorescent dyes onto ferrite nanoparticles during their synthesis from aqueous solution, J. Appl. Phys. 93 (10) (2003) 7569–7570.

[30] P.J. Borm, D. Robbins, S. Haubold, T. Kuhlbusch, H. Fissan, K. Donaldson, R. Schins, V. Stone, W. Kreyling, J. Lademann, The potential risks of nanomaterials: a review carried out for ECETOC, Part. Fibre Toxicol. 3 (1) (2006) 11.

[31] H. Hansson, F. Kaczala, M. Marques, W. Hogland, Photo-Fenton and Fenton oxidation of recalcitrant industrial wastewater using nanoscale zero-valent iron, Int. J. Photoenergy 2012 (2012).

[32] R. Crane, T. Scott, Nanoscale zero-valent iron: future prospects for an emerging water treatment technology, J. Hazard Mater. 211 (2012) 112–125.

[33] R.F.P. Nogueira, A.G. Trovo, M.R.A. da Silva, R.D. Villa, M.C. de Oliveira, Fundaments and environmental applications of Fenton and photo-Fenton processes, Quim. Nova 30 (2) (2007) 400–408.

[34] O. Rozas, D. Contreras, M.A. Mondaca, M. Pérez-Moya, H.D. Mansilla, Experimental design of Fenton and photo-Fenton reactions for the treatment of ampicillin solutions, J. Hazard Mater. 177 (1-3) (2010) 1025–1030.

[35] B. Ohtani, Revisiting the fundamental physical chemistry in heterogeneous photocatalysis: its thermodynamics and kinetics, Phys. Chem. Chem. Phys. 16 (5) (2014) 1788–1797.

[36] Y. Chen, S. Yang, K. Wang, L. Lou, Role of primary active species and TiO2 surface characteristic in UV-illuminated photodegradation of Acid Orange 7, J. Photochem. Photobiol. Chem. 172 (1) (2005) 47–54.

[37] M. Kooti, S. Gharineh, M. Mehrkhah, A. Shaker, H. Motamedi, Preparation and antibacterial activity of $CoFe_2O_4/SiO_2$/Ag composite impregnated with streptomycin, Chem. Eng. J. 259 (2015) 34–42.

[38] M. Kooti, P. Kharazi, H. Motamedi, Preparation, characterization, and antibacterial activity of $CoFe_2O_4$/polyaniline/Ag nanocomposite, J. Taiwan Inst. Chem. E 45 (5) (2014) 2698–2704.

[39] R. Vidya, K. Venkatesan, Preparation and characterization of zinc ferrite ($ZnFe_2O_4$) nanoparticles using self-propagated combustion route and evaluation of antimicrobial activity, Res. J. Pharmaceut. Biol. Chem. Sci. 6 (1) (2015) 537–542. ISSN: 0975-8585.

[40] M. Hashim, S.E. Shirsath, S. Meena, R. Kotnala, A. Parveen, A.S. Roy, S. Kumar, P. Bhatt, R. Kumar, Investigation of structural, dielectric, magnetic and antibacterial activity of Cu–Cd–Ni–FeO_4 nanoparticles, J. Magn. Magn Mater. 341 (2013) 148–157.

[41] J. Sawai, Quantitative evaluation of antibacterial activities of metallic oxide powders (ZnO, MgO and CaO) by conductimetric assay, J. Microbiol. Methods 54 (2) (2003) 177–182.

[42] S. Xavier, H. Cleetus, P. Nimila, S. Thankachan, R. Sebastian, E. Mohammed, Structural and antibacterial properties of silver substituted cobalt ferrite nanoparticles, Res. J. Pharmaceut. Biol. Chem. Sci. 5 (5) (2014) 364–371. ISSN: 0975-8585.

[43] Y.-C. Chung, Y.-P. Su, C.-C. Chen, G. Jia, H.-l. Wang, J.G. Wu, J.-G. Lin, Relationship between antibacterial activity of chitosan and surface characteristics of cell wall, Acta Pharmacol. Sin. 25 (7) (2004) 932–936.

[44] F.F. Arhin, G.A. McKay, S. Beaulieu, I. Sarmiento, T.R. Parr Jr., G. Moeck, Time–kill kinetics of oritavancin and comparator agents against Streptococcus pyogenes, Int. J. Antimicrob. Agents 34 (6) (2009) 550–554.

[45] C. Hellio, A.M. Pons, C. Beaupoil, N. Bourgougnon, Y. Le Gal, Antibacterial, antifungal and cytotoxic activities of extracts from fish epidermis and epidermal mucus, Int. J. Antimicrob. Agents 20 (3) (2002) 214–219.

[46] K. Maaz, A. Mumtaz, S. Hasanain, A. Ceylan, Synthesis and magnetic properties of cobalt ferrite (CoFe2O4) nanoparticles prepared by wet chemical route, J. Magn. Magn Mater. 308 (2) (2007) 289–295.

[47] G. Vaidyanathan, S. Sendhilnathan, R. Arulmurugan, Structural and magnetic properties of Co1− $xZnxFe_2O_4$ nanoparticles by co-precipitation method, J. Magn. Magn Mater. 313 (2) (2007) 293–299.

[48] J.S. Sagu, K. Wijayantha, A.A. Tahir, The pseudocapacitive nature of $CoFe_2O_4$ thin films, Electrochim. Acta 246 (2017) 870–878.
[49] M. Kurian, S. Thankachan, D.S. Nair, E. Aswathy, A. Babu, A. Thomas, B.K. Kt, Structural, magnetic, and acidic properties of cobalt ferrite nanoparticles synthesised by wet chemical methods, J. Adv. Ceram 4 (3) (2015) 199–205.
[50] I. Gul, A. Maqsood, Structural, magnetic and electrical properties of cobalt ferrites prepared by the sol–gel route, J. Alloys Compd. 465 (1-2) (2008) 227–231.
[51] M. Sangmanee, S. Maensiri, Nanostructures and magnetic properties of cobalt ferrite ($CoFe_2O_4$) fabricated by electrospinning, Appl. Phys. A 97 (1) (2009) 167–177.
[52] K. Kombaiah, J.J. Vijaya, L.J. Kennedy, M. Bououdina, B. Al Najar, Self heating efficiency of $CoFe_2O_4$ nanoparticles: a comparative investigation on the conventional and microwave combustion method, J. Alloys Compd. 735 (2018) 1536–1545.
[53] X. Liu, S. Liu, M.-G. Han, L. Zhao, H. Deng, J. Li, Y. Zhu, L. Krusin-Elbaum, S. O'Brien, Magnetoelectricity in $CoFe_2O_4$ nanocrystal-P (VDF-HFP) thin films, Nanoscale Res. Lett. 8 (1) (2013) 374.
[54] Z. Mohammadi, N. Attaran, A. Sazgarnia, S.A.M. Shaegh, A. Montazerabadi, Superparamagnetic cobalt ferrite nanoparticles as T_2 contrast agent in MRI: in vitro study, IET Nanobiotechnol. 14 (5) (2020) 396–404.
[55] M. Ravichandran, G. Oza, S. Velumani, J.T. Ramirez, F. Garcia-Sierra, N.B. Andrade, M.A. Garza-Navarro, D.I. Garcia-Gutierrez, R. Lara-Estrada, E. Sacristán-Rock, Cobalt ferrite nanowhiskers as T_2 MRI contrast agent, RSC Adv. 5 (22) (2015) 17223–17227.
[56] D. Das, B.C. Nath, P. Phukon, S.K. Dolui, Synthesis of ZnO nanoparticles and evaluation of antioxidant and cytotoxic activity, Colloids Surf. B Biointerfaces 111 (2013) 556–560.
[57] Y. Gao, M.A.V. Anand, V. Ramachandran, V. Karthikkumar, V. Shalini, S. Vijayalakshmi, D. Ernest, Biofabrication of zinc oxide nanoparticles from Aspergillus Niger, their antioxidant, antimicrobial and anticancer activity, J. Cluster Sci. 30 (4) (2019) 937–946.
[58] M. Abd Elkodous, G.S. El-Sayyad, A.M. Mia, I.Y. Abdelrahman, F.M. Mosallam, M. Gobara, A.I. El-Batal, Fabrication of ultra-pure anisotropic zinc oxide nanoparticles via simple and cost-effective route: implications for UTI and EAC medications, Biol. Trace Elem. Res. (2019).
[59] H.K. Abdelhakim, E. El-Sayed, F.B. Rashidi, Biosynthesis of zinc oxide nanoparticles with antimicrobial, anticancer, antioxidant and photocatalytic activities by the endophytic Alternaria tenuissima, J. Appl. Microbiol. 128 (6) (2020) 1634–1646.
[60] E.-S.R. El-Sayed, H.K. Abdelhakim, Z. Zakaria, Extracellular biosynthesis of cobalt ferrite nanoparticles by Monascus purpureus and their antioxidant, anticancer and antimicrobial activities: yield enhancement by gamma irradiation, Mater. Sci. Eng. C 107 (2020) 110318.
[61] E.-S.R. El-Sayed, H.K. Abdelhakim, A.S. Ahmed, Solid-state fermentation for enhanced production of selenium nanoparticles by gamma-irradiated Monascus purpureus and their biological evaluation and photocatalytic activities, Bioproc. Biosyst. Eng. (2020) 1–13.